Low Resolution Three Dimensional Reconstruction of CMEs Using Solar Mass Ejection Imager (SMEI) Data

Bernard V. Jackson*, Andrew Buffington**, P. Paul Hick***, and Cindy X..Wang****
Center for Astrophysics and Space Sciences, University of California, San Diego

ABSTRACT

White-light Thomson scattering observations from the Solar Mass Ejection Imager (SMEI) have recorded the inner heliospheric response to many CMEs. Here we detail how we determine the extent of several CME events in SMEI observations (including those of 28 May 28 and 28 October, 2003). We show how we are able to measure these events from their first observations as close as 20° from the solar disk until they fade away in the SMEI 180° field of view. We employ a 3D reconstruction technique that provides perspective views from outward-flowing solar wind as observed at Earth. This is accomplished by iteratively fitting the parameters of a kinematic solar wind density model to the SMEI white light observations and to Solar-Terrestrial Environment Laboratory (STELab), interplanetary scintillation (IPS) velocity data. This 3D modeling technique enables separating the true heliospheric response in SMEI from background noise, and reconstructing the 3D heliospheric structure as a function of time. These reconstructions allow both separation of the 28 October CME from other nearby heliospheric structure and a determination of its mass. Comparisons with LASCO for individual CMEs or portions of them allow a detailed view of changes to the CME shape and mass as they propagate outward.

Keywords: Coronal mass ejections, CME-corotating region interactions, tomography, 3D reconstructions

1. INTRODUCTION

The Solar Mass Ejection Imager (SMEI)[1,2] was launched on January 6, 2003. The instrument (Figure 1a) consists of three baffled cameras whose 3°×60° fields of view are aligned in the long dimension to achieve a combined ~160° wide field of view that scans most of the sky every 102-minute orbit (Figure 1b). The cameras are designed to view the heliosphere in Thomson scattered light at one-degree spatial resolution. Data from each four-second camera exposure (Figure 2a) are used to input to a global mosaic sky map (Figure 2b) comprised of approximately 4500 images.

For the bulk of the data (in 'science mode' with CCD pixels combined into 4×4 pixel averages) the angular resolution in these image frames is ~0.2°. Camera 3 (which views closest to the Sun) regularly operates in 2×2 mode and thus has a twice finer angular resolution than the other two cameras. These images are stored and regularly telemetered to the ground employing a lossless Rice compression algorithm. Currently, SMEI returns about three gigabytes of data each day. The design specification for SMEI states that the SMEI instrument will provide a 0.1% photometric result in one square degree of sky at an elongation of 90° from the Sun in a single orbital sky map. This will provide a signal to noise of about 10% for dense heliospheric structures at this elongation[2]. We have found that at locations in the sky map where there are few high energy particle fluxes and no aurora light, that SMEI exceeds this specification by about a factor of two[3].

SMEI is the first true spaceborne white-light 'heliospheric imager'. It has much better sky coverage, spatial resolution and time cadence than previous remote sensing instruments (*i.e*., HELIOS), and permits continuous imaging sequences, thus providing a global view of heliospheric structures as they move across the sky over a wide range of solar elongations. The SMEI data provide a new, unique perspective on heliospheric observations of solar disturbances.

SMEI is currently the best design we know for operation near Earth on a spacecraft not specifically designed for the instrument, and where the Moon and stray light from spacecraft bus appendages have the potential to overwhelm the faint brightness signal from heliospheric electrons. The overall SMEI design has progressed over a period of nearly two decades[4-8,1,2].
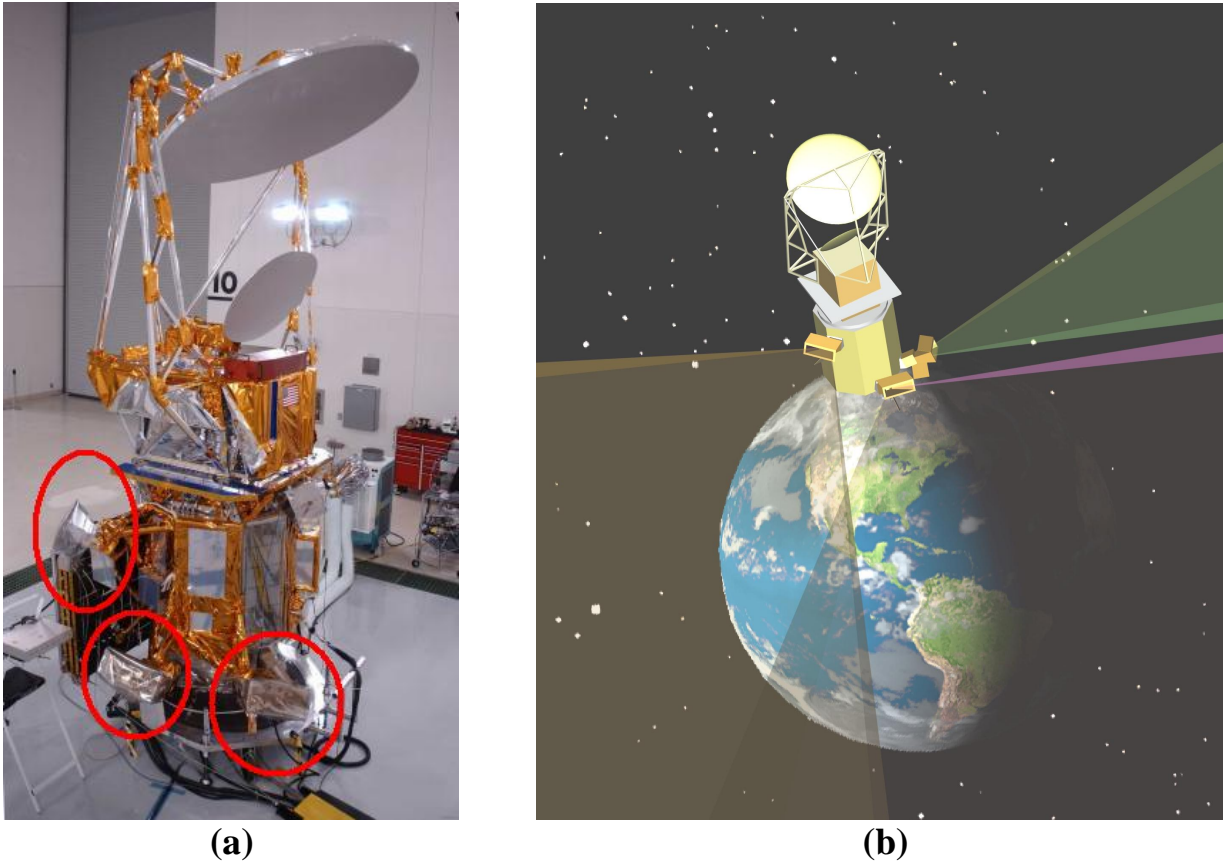
(a)   **(b)**

Figure 1. **(a)** The Coriolis spacecraft with the Solar Mass Ejection Imager (SMEI) instrument and the *Windsat* antenna prior to launch from Vandenberg AFB. The three SMEI camera baffles (circled) are seen on the lower portion of the spacecraft. **(b)** SMEI in its polar orbit at 840 km with an orbital inclination of 98°. SMEI looks away from the Earth at 30° from the local horizontal to avoid sunlight reflected from the Earth and from the *Windsat* antenna. The combined fields of view of the three cameras (shown as shaded cones) cover over 160° of sky.

There have been numerous attempts to reconstruct coronal structures in the corona and heliosphere in 3D. These techniques, reviewed elsewhere[9-13], have been motivated by attempts to determine heliospheric structure morphology in order to determine their physics, their dynamics and most recently to forecast their arrival at Earth using remote sensing techniques.

Rotational tomography of stationary solar structures (streamers) using coronagraph observations have been presented by Wilson[14], Jackson[15], and by Zidowitz *et al*.[16]. More recently, Jackson *et al*.[17,18] presented results that show heliospheric 3-dimensional reconstructions from outward plasma flow alone. These "time-dependent" tomographic analyses have been used to determine and successfully forecast the Earth arrival of both heliospheric corotating structures and mass ejections from ground-based interplanetary scintillation (IPS) observations and now SMEI brightness data.

Section 2 details the motivation behind the SMEI instrument that includes the real-time analysis program that is currently operated at UCSD to analyze interplanetary scintillation (IPS) observations, data that are used to augment the UCSD SMEI data analysis and map heliospheric structures in 3D. Section 3 describes SMEI image data processing and its current status at UCSD. Section 4 gives examples of this analysis and compares these tomographic models to ACE *in situ* observations and to coronagraph observations of the same CME. We conclude in Section 5.
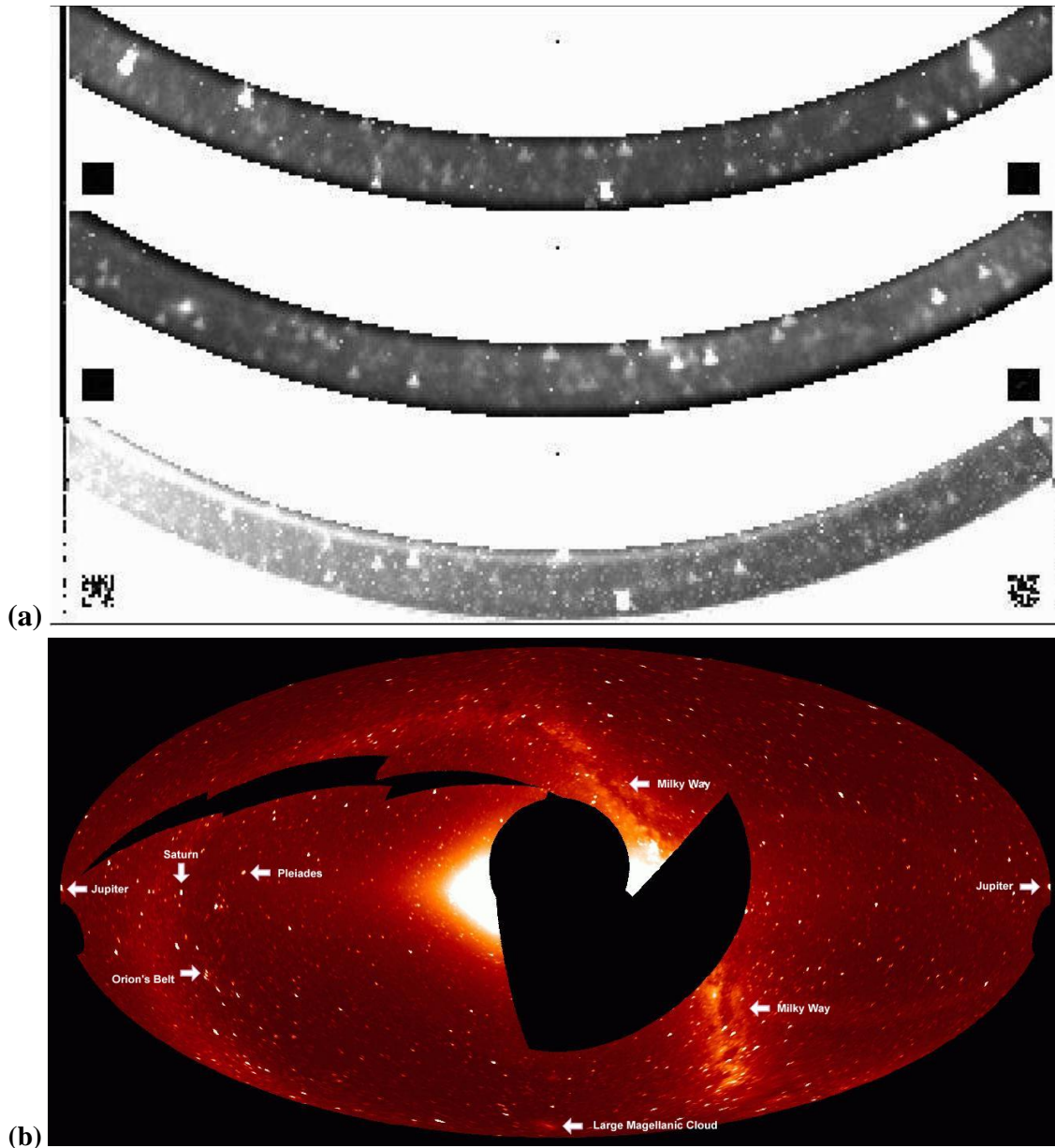
Figure 2a. 3°×60° image frames from each of the three SMEI cameras. Camera 1 (top) views farthest from the Sun; camera 3 (bottom) closest, with the Sun towards the left in each frame. **(b.)** 'First light' Hammer-Aitoff projection of the sky built as a composite from SMEI data frames over a 102-minute orbit around Earth. Various bright features are labeled. Blank regions were excluded because they were not accessible to the cameras during the orbit, were too close to the Sun and thus too bright, or contaminated by high-energy particle enhancements (the slash across the upper left side of the skymap image). See: **http://cassfos02.ucsd.edu/solar/smei_new/smei.html**, and other links for more images and a SMEI archive of orbit by orbit difference maps.

2. HELIOSPHERIC REMOTE SENSING

Heliospheric remote sensing observations provide one of very few means of observing structures in the solar wind located between the immediate solar environment (as observed by coronagraphs) and their arrival at 1 AU (as observed by near-Earth *in situ* instruments). These remote sensing data probe the global extent of the solar wind over a large range of solar elongations. They also extend across the high-latitude regions (the solar poles), difficult of access by other

means. Past UCSD work has extensively employed heliospheric remote sensing to study the physics of structures in the solar wind as they move out into the heliosphere.

IPS observations, measuring meter-wavelength intensity variations of point radio sources, are one source of heliospheric remote sensing information. These are caused by small-scale (~200 km) heliospheric density variations along the line of sight to a radio source[19,20]. IPS observations from the Cambridge, UK, array[21] show structures that can be classified either as corotating or as detached from the Sun[22,23]. We have developed 3D techniques to analyze these[24,25,9,10]. In collaboration with colleagues at the Solar-Terrestrial Environment Laboratory (STELab) at Nagoya University, Toyokawa, Japan, UCSD currently operates a real-time, web-based system that forecasts solar wind conditions near Earth (see **http://cassfos02.ucsd.edu/solar/forecast/index_v_n.html**).

SMEI remote-sensing observations have obvious potential for studying propagation and evolution of heliospheric structures as they interact with each other and the ambient solar wind. However, as with coronagraph and IPS data, interpretation is complicated because each observation is a line-of-sight integration. Apparent brightness distribution and 'plane-of-the-sky' motion depend on an *a priori* unknown 3D distribution of outward moving solar wind material at uncertain locations relative to Sun and Earth.

One can resolve the ambiguity by assuming the structures are all located in the plane of the sky. This provides useful information about persistent (corotating) solar wind structures[26]. However, when a transient structure such as a heliospheric response to a CME is followed across a wide range of solar elongations (as expected from SMEI), the plane-of-the-sky assumption cannot be correct over the whole period of observation. In addition, the structure in general extends along a significant portion of the line of sight at all times, casting further doubt on this plane-of-the-sky assumption.

These considerations led us to develop an analysis tool that directly addresses the line-of-sight problem. It explicitly takes into account the 3D extent of heliospheric structures including the fact that the contribution is dominated by material closest to the Sun, but without explicit assumptions about the distribution of velocity and density along these lines of sight. Thus, it reconstructs 3D solar wind structures from remote sensing data gathered at a single location, as with SMEI. This technique is necessary to tap the full heliospheric-imager SMEI potential, and enable it as a predictive tool for space weather purposes.

This analysis is a general methodology to use views of a structure from many different perspectives to reconstruct its 3D shape. Usually heliospheric remote-sensing observations are available from only a single viewing location, *i.e.*, from Earth. Perspective information in this case comes from solar rotation and outflow in the solar wind. Assuming that structures change little except for corotation within one solar rotation, rotation alone yields sufficient information for reconstruction of the quiet corona[27,28,16,29,30] and the corotating solar wind.

However, transients such as CMEs evolve on much shorter time scales, hours to days. For observations covering a wide range of solar elongations, heliospheric structures are seen from widely different directions as they move past Earth. This feature, essentially absent in coronagraph data, allows 3D reconstruction using heliospheric data such as from SMEI, for time-dependent reconstruction of transient structures.

3. SMEI IMAGE FRAME PROCESSING

Telemetry from SMEI is relayed from the ground stations to the AFRL SMEI data processing center, where data packets are concatenated, individual camera data frames are decompressed, and combined with an assigned set of spacecraft quaternions (spacecraft pointing derived from a star tracker). The resulting CCD data frames are placed on an AFRL FTP site at Sacramento Peak Observatory, transferred to UCSD and written onto DVDs. UCSD maintains a database of these SMEI image frames in near real time on a local server. Sacramento Peak also maintains an archive of original SMEI images. Figure 2a shows a set of simultaneous 4-second exposure 'image frames' from these three cameras.

Both AFRL and UCSD have independently developed analysis sequences to reduce individual SMEI image frames whose final product is a heliospheric sky map for every orbit of data. Image frames from a complete orbit are combined into composite sky maps (Figure 2b) which are generally displayed with an angular resolution of 1° at the orbital time cadence of 102 minutes. The AFRL analysis sequence uses similar steps to those at UCSD, but is specifically crafted to

demonstrate the feasibility of detecting and tracking solar mass ejections in near real time. The AFRL analysis is focused on an expedient presentation of SMEI data in the form of 2D sky maps (Figure 2b), and these are presented in near real time to the SMEI team.

The UCSD sequence of data analysis steps differs most from that at AFRL at the point where a high-resolution grid is formed. UCSD uses a HTM grid system[31] of ~5 times finer angular resolution than that used by AFRL, and as this grid is formed an algorithm removes high-energy particle hits and space debris from the data. This process removes most positive and negative error contributions such as these from individual SMEI image frames; it oftentimes allows nearly complete recovery of photometric SMEI data from particle hits on the CCD as SMEI passes through the Earth's auroral oval regions and the South Atlantic Anomaly. A lesser resolution (~0.2° in latitude and longitude) sidereal sky map complete with stellar signals is then recovered from the finely divided HTM grid for use and presentation in different coordinate projections - Sidereal, Fisheye and all-sky Hammer-Aitoff.

The UCSD SMEI analysis[2] is driven by the requirement that the sky maps approach as close as possible to full photometric and angular resolution design limits of SMEI. This enables the best quantitative analysis of the SMEI data. The promise of modeling heliospheric density structure using 3D reconstruction techniques is foremost here (see next section).

SMEI sky maps should permit observing heliospheric structures that persist for a significant fraction of a solar rotation. This enables the study of slow (corotating) as well as rapidly moving transient features. Thus, sky maps must retain a constant temporal base over time periods of as many weeks as possible, to measure both corotating structures as well as fast-moving transient structures. The 3D reconstructions require optimal removal of non-heliospheric and zodiacal artifacts but also that as little as possible of the Thomson-scattered signal be inadvertently removed in the process.

Since light from the sidereal sky (stars, the Milky Way, nebulae, galaxies) is about 100× brighter than the variable Thomson-scattered signal, this background must be removed from orbit-to-orbit SMEI sky maps. The simplest way to do this is by subtracting one Sun-centered sky map from the next ('running differences'); here only the change in the heliospheric signal, due to motion of the structures, over the orbital time period (Δt = 102 minutes), remains. Tappin *et al.*[32] use this method to study the heliospheric response to a halo CME originating on the Sun on May 28, 2003, and observed by SMEI on May 29. Several hundred transient events have been observed by this method in the SMEI observations to date, and more than half of these can be first identified as CMEs in the SOHO LASCO coronagraph data. Such difference maps are useful for real-time presentation of SMEI data, and adequate for identifying and even tracking disturbances distant from Earth. However this simple analysis sacrifices the wealth of more slowly varying features present in SMEI data. They also contain regions of positive and negative differences, complicating interpretation and a quantitative analysis.

Alternatively, a sidereal sky map averaged over many orbits close in time to a heliospheric event can be subtracted. This method preserves more heliospheric signal by effectively enlarging the base time scale Δt. Figures 3a and 3b show examples of such difference sky maps plotted in Sun-centered ecliptic coordinates for the 29 May 2003 CME event (see also Jackson *et al.*[2]) for two selected orbits. Figure 4 is the time series variation of heliospheric signal at three selected locations. Here, to first order, we see that SMEI instrumental and sidereal-background changes have been rendered small relative to the actual heliospheric plasma signals.

Our current analysis provides a stable baseline over several weeks, without sacrificing angular resolution. This provides a calibrated data set sufficient for the 3D analysis. The 3D results in turn will refine SMEI images, which can be presented from any desired viewing location; the original sky maps are often contaminated by troublesome backgrounds and portions of these are sometimes further swamped by bright auroral light. Extrapolating across these regions and removing contaminant signals is best accomplished as we do in IPS sky maps. Here, sky map outages and contaminant signals are modeled away using a realistic 3D solar wind model iteratively fit to the data, both removing the contaminated regions and extrapolating across them. The best editing retains only the heliospheric signal in the sky maps. Figures 3c and 3d show samples of this technique's ability to refine 2D SMEI sky maps. Ultimately, the optimum removal of the sidereal and zodiacal sky map contributions rests on forming an average of background light over a baseline of a year or more, together with individual-star subtraction for variables brighter than about 6th magnitude.
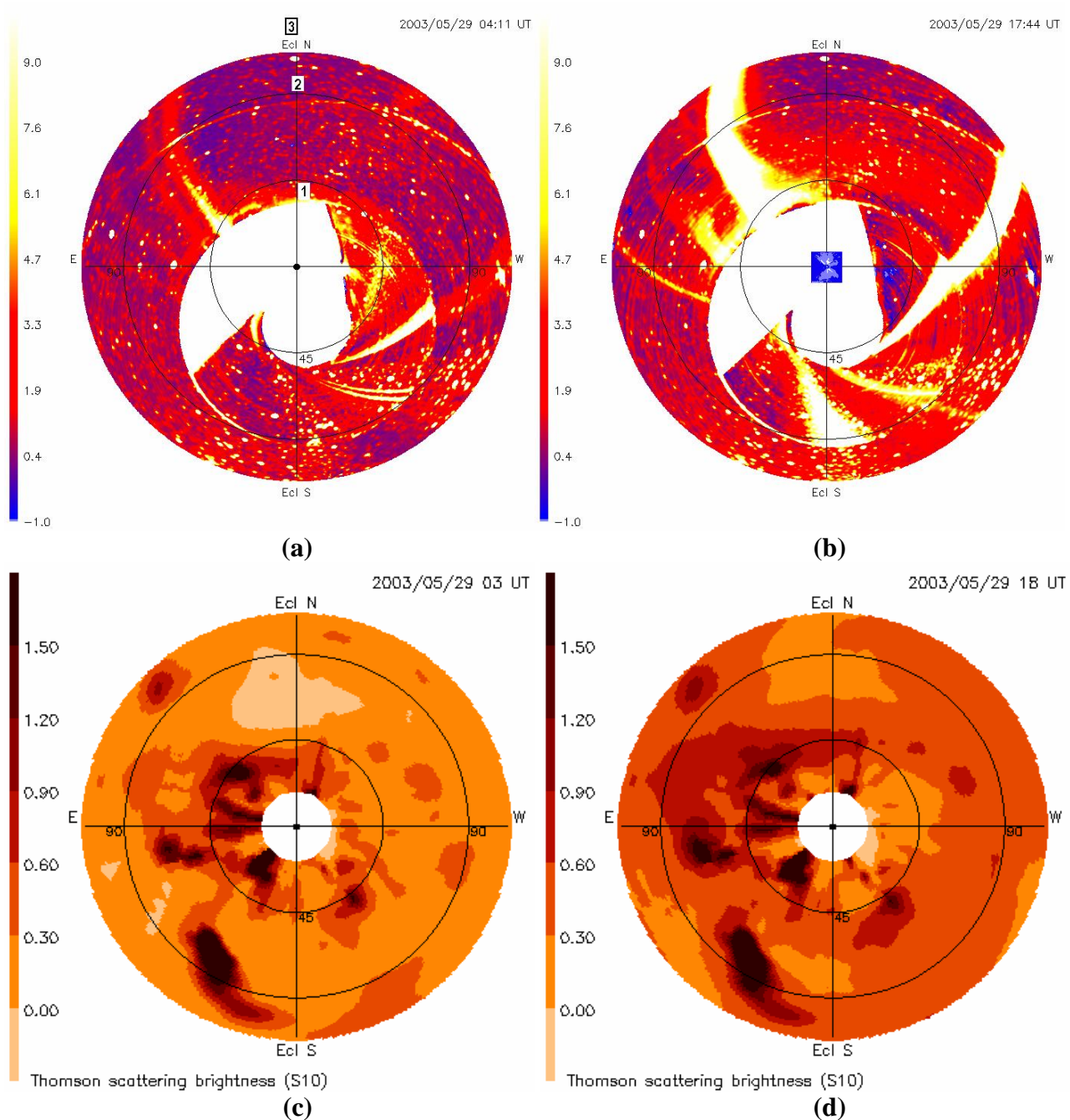
Figure 3. SMEI 'fisheye' skymap images of the heliospheric response to the May 28, 2003 CME observed to 'halo' the Sun in LASCO observations and in SMEI observed beyond 45° elongation in the first image set and to have begun to engulf the Earth at 90° elongation in the second at the times indicated. **a)** and **b)** Direct SMEI sky map images on 29 May, 2003. Shown are two orbits of data differenced from an 8-orbit average for SMEI cameras 1, 2 and 3. The white regions in the sky maps that extend roughly outward from the center are primarily locations where auroral light is too bright to provide a photometric signal. The data were smoothed using a 1° Gaussian filter. The specks in each image are stellar signals – mostly bright stars that have changed brightness over the observation interval. Brightness is in SMEI camera analog to digital units (ADU). One S10 is approximately 0.4 ADU. A LASCO C3 coronagraph image is inserted in the top right map for scale. Numbered locations 1-3 on map **a)** indicate the regions shown as time series in Figure 4. **c) and d)** The approximate same images showing far more features and the halo enhancement surrounding Earth are obtained from time series modeling as described later in the text using SMEI data from cameras 1, 2, and 3. Brightness is given in S10 normalized to an r^{-2} density falloff relative to the 90° elongation circle.
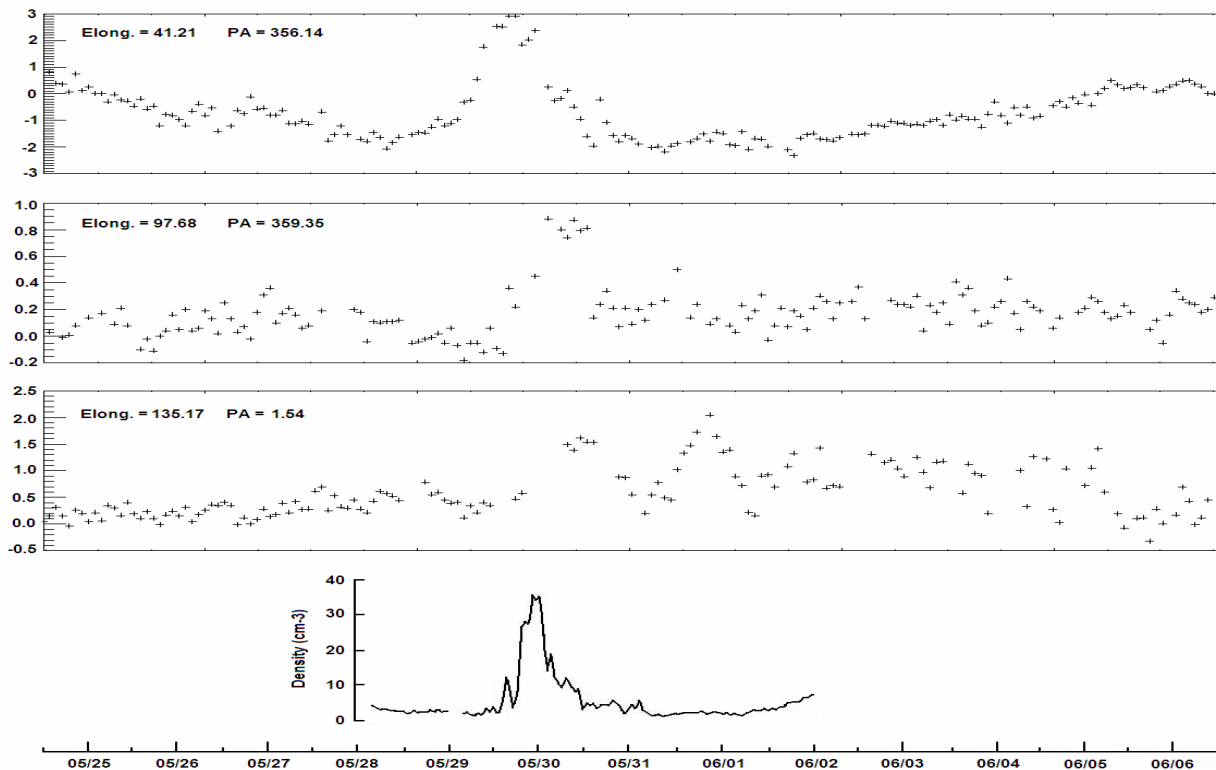
Figure 4. **(top)** Time series from three selected sidereal locations using data from 183 SMEI orbits from 24 May – 6 June 2003 at the approximate elongation and ecliptic position angles indicated during the passage of the 'halo' CME response of May 28, 2003. The enhancement is first seen midday on 29 May in these sequences. The disturbance shows as a broad peak present in about ten orbits of data. A 100-orbit running mean baseline has been removed from each time series to eliminate long term changes in them such as those from inaccurately modeled zodiacal light not eliminated by background subtraction. The time series have been chosen so that the square degree they measure are not located within a 1.5° of a star brighter than 6th magnitude, and have been edited of auroral light. **(bottom)** ACE *in situ* solar wind proton density time series (hourly averages) show an associated enhancement reaching Earth midday on 29 May, and continuing into 30 May.

4.   HELIOSPHERIC 3D RECONSTRUCTION

Presently, our 3D reconstruction incorporates a purely kinematic solar wind model. Given the velocity and density of an inner boundary (the 'source surface'), a fully 3D solar wind model best fitting the observations follows, by assuming radial outflow and enforcing conservation of mass and mass flux[9]. Best fit is achieved iteratively: if the 3D solar wind at large solar distances does not match the overall observations, the source surface values are changed to reduce the deviations to a desired small value.

We have employed this technique to successfully analyze CME-associated structures using IPS and SMEI Thomson scattering observations. Figure 5a is an example of a 3D heliospheric analysis using SMEI Thomson scattering brightness and Nagoya IPS velocity data and digital time steps of 1/2 day and resolutions in latitude and longitude of 7.5°. Different Gaussian filters are used for the two data sets and they limit the size of structures observed more than the digital resolution[13]. Figure 5b shows a preliminary comparison with ACE density data for this time interval and Figure 5c shows the correlation.
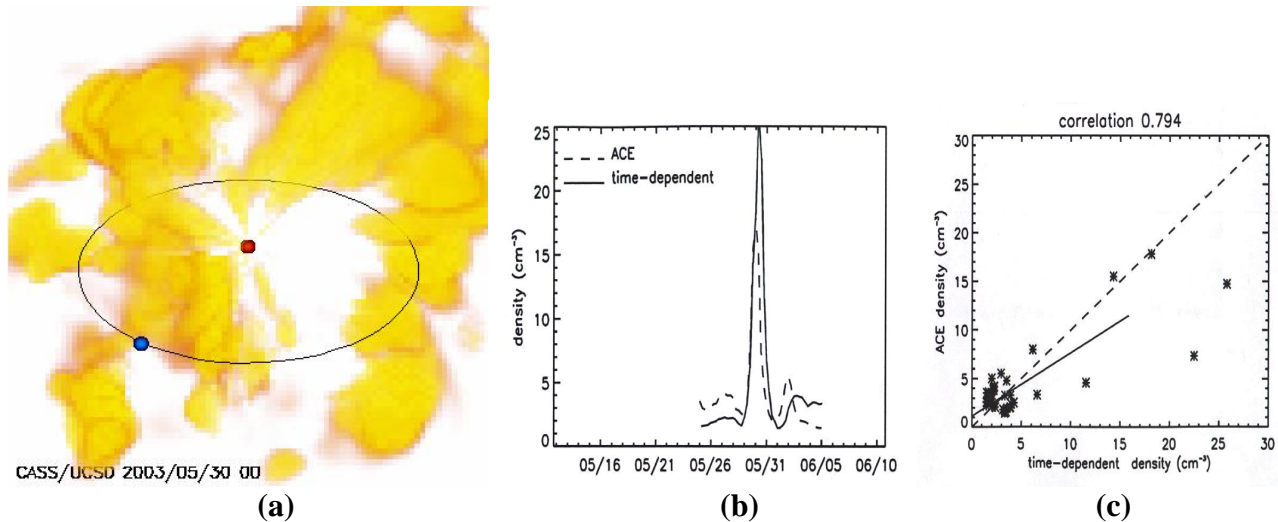
Figure 5. 3D reconstruction of the May 28 Halo CME as it is about to hit Earth. For animations of the remote views in this figure see: **http://cassfos02.ucsd.edu/solar/smei_new/analysis.html**. **(a)** 3D reconstruction using SMEI brightness and IPS velocity data. A view from 3 AU, 30° above the ecliptic plane at the time indicated is shown. The digital angular resolution is 7.5° × 7.5° in latitude and longitude. The 3D reconstructions have a digital temporal cadence of one-half day. The main structure near Earth is associated with the halo CME observed by LASCO on May 28, 2003, and shows that the density enhancement of the CME that hits Earth in this event is a relatively small density feature in the overall CME structure that leaves the Sun. **(b)** Time series plot of the density at Earth extracted from the reconstruction in comparison with Advanced Composition Explorer (ACE) observations. ACE observations are combined into 12-hour averages matching the temporal and spatial resolutions of the SMEI 3D brightness reconstruction. The correlation has been limited to data times within about 5 days of the event. These resolutions are more coarse than the 1° × 1° latitude, longitude resolutions at orbital cadences that may ultimately be available from the SMEI data sequences. **(c)** Correlation of the 3D reconstructed model with ACE 12-hour averaged data.

Thomson scattering brightness measures density much closer than the IPS 'g-level' density proxy in this IPS 3D reconstruction. Thus HELIOS-photometer 3D reconstruction analyses[12] are free of this difficulty, but present preliminary SMEI results show <u>these</u> data are far more precise, and of course much more abundant. The 3D reconstruction analysis must also take into account, in addition to the observed time-varying signal, that there is an unknown steady background component. An estimate of this is included by relating model densities to *in situ* observations, near Earth, of the sum of the variable and steady-state parts of the solar wind. SMEI cameras are currently being calibrated using known G-star brightness, and this calibration should be available within a few months, to an estimated 0.5% for all SMEI cameras (we currently claim ~10% calibration). The time series obtained from the SMEI 3D reconstruction for the May 28 halo CME response currently produces a density peak at the same location in time as observed by the ACE spacecraft, and well within a factor of two amplitude of the *in situ* result (Figure 5b). The SMEI angular and time resolution (shown in Figure 5 in preliminary low-resolution analysis) will in principle allow us to improve density results to approximately 10 times better than IPS spatial and time dimension 3D reconstructed resolutions.

Even though the 3D reconstruction can be used when only SMEI's Thomson scattering brightness is available, better results are obtained when IPS velocity data (the only remote sensing data to provide direct measurements of solar wind speed) are included. The very best 3D reconstruction results will be reached when SMEI 0.1% differential photometric precision is combined with velocity data. Currently STELab provides IPS velocities in real time most of the year, and these data are available for the SMEI data reduction as well as study the difference in the data sets.

These data sets can be compared with the LASCO coronagraph observations and the results go a long way toward certifying the SMEI data analysis. These analyses show which portions of CMEs observed in a coronagraph move outward into the interplanetary medium and where individual features seen in the coronagraph images are relative to the plane of the sky. Figure 6 shows a LASCO C3 coronagraph image of the October 28, 2003 halo CME. In this image there is a clear very dense loop-like structure seen moving outward to the south of the Sun, and a halo that contains a slight enhancement of mass to the solar northeast. The dense structure persists in the SMEI data reconstructions shown in Figure 7 as a dominant feature south of the Sun that is about 20° from the plane of the sky. The halo portion of the event is also observed in SMEI, and the reconstruction shows dense material that moves outward to engulf the Earth

somewhat later than the very rapid shock response that reached Earth from the event about 20 hours following its eruption from the Sun. In the reconstruction, the slightly enhanced portion of the ejection observed to the solar northwest is shown to be a far more dense structure, but simply very far from the plane of the sky when observed in LASCO, and this accounts for its relative lack of brightness in these data. The reconstructions show that the northeast part of the solar event is linked by a thin bridge of denser material all the way from the north of the Sun to down to and including the dense loop-like structure to the south of the Sun. Mass values can be derived from the LASCO C3 coronagraph for this event (Vourlidas, private communication, 2004), and corrected for plane of sky effects by using the SMEI 3D results. The 3D masses measured by SMEI for the same features are larger by factors of ~2 for the lower loop-like portion of the event and ~3 for the upper portion that engulfs Earth. This indicates these structures may likely have gained significant mass in the interplanetary medium.
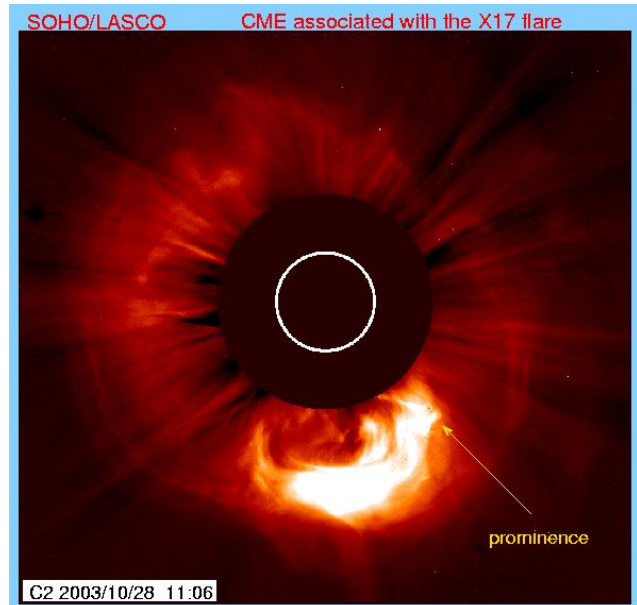

Figure 6. LASCO C2 observations of the October 28, 2003 CME. Most of the early CME response 'halos' the Sun and is associated with an X17.2 flare at S16 E09 that commences at 10:36 UT October 28. The large eruption to the south associated with a solar prominence (indicated) is also viewed to move outward over time to the south in LASCO images.

5. CONCLUSION

The Solar Mass Ejection Imager (SMEI) has been operating successfully for more than two and a half years. Here we have detailed how we determine the extent of several CME events in SMEI observations (including those of 28 May 2003 and 28 October, 2003). We show how we are able to measure these events from their first observations as close as 20° from the solar disk until they fade away in the SMEI ~180° field of view by employing a 3D reconstruction technique that provides perspective views from outward-flowing solar wind as observed from Earth. This 3D modeling technique enables separating the true heliospheric response in SMEI from background noise, and reconstructing the 3D heliospheric structure as a function of time. Comparisons with LASCO for individual CMEs or portions of them allow a detailed view of changes to the CME shape and mass as they propagate outward.

Although these reconstructions allow separation of the 28 October CME from other nearby heliospheric structure, they are preliminary in that they use only approximately 1/25th of the numbers of lines of sight from SMEI, and only partially account for the long-term base that must be subtracted from the heliospheric plasma variations. To utilize more lines of sight (that will allow a many-fold enhancement of the 3D reconstructions) will require significantly more computer resources than are now allocated to the reconstruction process, and the careful elimination of the effects of brighter stars in SMEI sky maps. To remove a longer-term base from the time series will require an accurate accounting of the zodiacal cloud and careful camera to camera calibration as sidereal sky locations cross SMEI camera boundaries.
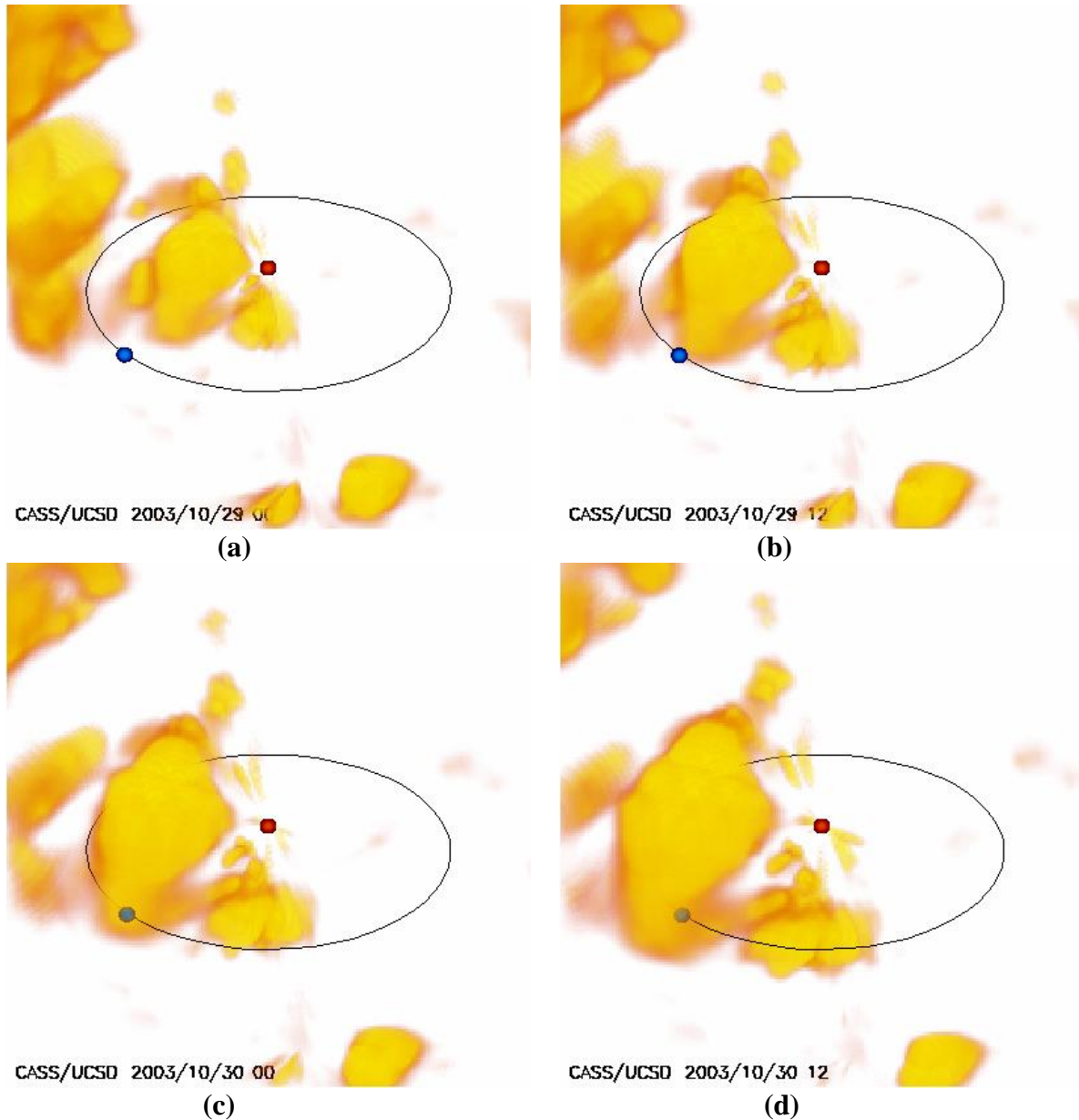
Figure 7. 3D reconstructions at four successive times of the heliospheric response to the October 28, 2003 CME as viewed from 3AU 30° above the ecliptic plane and ~45° west of the Sun-Earth line. The location of the Earth is indicated by a blue circle with the Earth's orbit viewed in perspective drawn as an ellipse. The Sun is indicated by a red dot. Densities are contoured between $10 - 30e^-$ cm^{-3} and have an r^{-2} density gradient removed from them. The fast structure moving to the solar northeast as observed from Earth is the dominant object here but contains only slightly more mass than the more dense structure to the south. The ejecta and loop associated with the solar prominence in the LASCO C2 view in Figure 6 are observed to the south of the Sun in these views.

REFERENCES

1.   C.J. Eyles, G.M. Simnett, M.P. Cooke, B.V. Jackson, A. Buffington, P.P. Hick, N.R. Waltham, J.M. King, P.A. Anderson, and P.E. Holladay, The Solar Mass Ejection Imager (SMEI), *Solar Phys.*, **217**, 319, 2003.
2.   B.V. Jackson, A. Buffington, P.P. Hick, R.C. Altrock, S. Figueroa, P.E. Holladay, J.C. Johnston, S.W. Kahler, J.B. Mozer, S. Price, R.R. Radick, R. Sagalyn, D. Sinclair, .G.M. Simnett, C.J. Eyles, M.P. Cooke, S.J. Tappin,

T. Kuchar, D.Mizuno, D.F. Webb, P.A. Anderson, S.L. Keil, R.E. Gold, and N.R. Waltham, The Solar Mass Ejection Imager (SMEI) Mission, *Solar Phys.* **225**, 177, 2004.

3. A. Buffington, D.L. Band, B.V. Jackson, P.P. Hick, and A.C. Smith, A Search for Early Optical Emission at Gamma-Ray Burst Locations by the Solar Mass Ejection Imager (SMEI), *Astrophys. J.* (to be submitted).

4. B.V. Jackson, H.S. Hudson, J.D. Nichols, and R.E. Gold, Design Considerations for a "Solar Mass Ejection Imager" on a Rotating Spacecraft, in *Solar System Plasma Physics Geophysical Monograph*, **54**, J.H. Waite, Jr, J.L. Burch and R.L. Moore, eds., 291, 1989.

5. B. Jackson, R. Gold, and R. Altrock, R., The Solar Mass Ejection Imager, *Adv. in Space Res.*, **11**, 377, 1991.

6. B.V. Jackson, A. Buffington, P.L. Hick, S.W. Kahler, R.C. Altrock, R.E. Gold R.E., and D.F. Webb, The Solar Mass Ejection Imager, in *Solar Wind Eight*, D. Winterhalter, J.T.Gosling, S.R. Habbal, W.S. Kurth and M. Neugebauer, eds., AIP Conference Proceedings **382**, Woodbury, 536, 1995.

7. B.V. Jackson, A. Buffington, P.L. Hick, S.W. Kahler, G. Simnett, and D.F. Webb, D.F., The solar mass ejection imager, *Physics and Chemistry of the Earth*, **22**, No. 5, 441, 1997a.

8. S.L. Keil, R.C. Altrock, S.W. Kahler, B.V. Jackson, A. Buffington, P.L. Hick, G. Simnett, C. Eyles, D.F. Webb, and P. Anderson, The Solar Mass Ejection Imager (SMEI), Denver 96 "Missions to The Sun", *SPIE* **2804**, 78, 1996.

9. B.V. Jackson, P.L. Hick, M. Kojima, and A. Yokobe, Heliospheric Tomography Using Interplanetary Scintillation Observations 1. Combined Nagoya and Cambridge data, *J. Geophys. Res.*, **103**, 12,049, 1998.

10. M. Kojima, M., Tokumaru, H. Watanabe, A. Yokobe, A., Asai, K., Jackson, B.V. and Hick, P.L., 1998, Heliospheric Tomography Using Interplanetary Scintillation Observations 2. Latitude and Heliocentric Distance Dependence of Solar Wind Structure at 0.1-1 AU, *J. Geophys. Res.*, **103**, 1981.

11. B.V. Jackson, and P.P. Hick, Corotational tomography of heliospheric features using global Thomson scattering data, *Solar Phys.*, **211**, 344, 2002.

12. B.V. Jackson, P.P. Hick, and A. Buffington, Time-dependent tomography of heliospheric features using the three-dimensional reconstruction techniques developed for the Solar Mass Ejection Imager (SMEI), *Proc. SPIE, Waikoloa*, 22-28 August 2002, **4853**, 23, 2002.

13. B.V. Jackson, and P.P. Hick, "Three-dimensional tomography of interplanetary disturbances", in: Solar and Space Weather Radiophysics Current Status and Future Developments, D.G. Gary and C.U. Keller, eds., *ASSL* **314**, Kluwer, The Netherlands, 355, 2004.

14. D.C. Wilson, *NCAR Cooperative Thesis No. 40*, Ph.D. thesis to the University of Colorado, Boulder, Colorado, 1977.

15. B.V. Jackson, "A coronal hole equatorial extension and its relation to a high speed solar wind stream", *Topical Conference on Solar and Interplanetary Physics*, Tucson, Arizona,. 7, 12-15 January, 1977.

16. S. Zidowitz, B. Inhester, and A. Epple, Tomographic inversion of coronagraph images, in: Proc. Solar Wind Eight, D. Winterhalter, J.T.Gosling, S.R. Habbal, W.S. Kurth and M. Neugebauer (eds), *AIP Conference Proceedings* **382**, Woodbury, 165, 1995.

17. B.V. Jackson, A. Buffington, and P.P. Hick, A heliospheric imager for solar orbiter, Proc. of "Solar Encounter: The First Solar Orbiter Workshop", Puerto de la Cruz, Tenerife, Spain, 14-18 May 2001 (*ESA* **SP-493**, September 2001), 251, 2001.

18. B.V. Jackson , P.P. Hick and A. Buffington, Time-dependent tomography of heliospheric features using interplanetary scintillation (IPS) remote-sensing observations, *Proceedings of Solar Wind 10,* Pisa, June 17-21, 75, 2003.

19. A. Hewish, P.F. Scott, D. and Wills, Interplanetary scintillation of small diameter radio sources, *Nature*, **203**, 1214, 1964.

20. S. Ananthakrishnan, W.A. Coles, J.J. and Kaufman, Microturbulence in solar wind streams, *J. Geophys. Res.*, **85**, 6025, 1980.

21. Z. Houminer, Corotating plasma streams revealed by interplanetary scintillation, *Nature Phys. Sci.*, **231**, 165, 1971.

22. A. Hewish, and S. Bravo, The sources of large-scale heliospheric disturbances, *Solar Phys.*, **106**, 185, 1986

23. K.W. Behannon, L.F. Burlaga, and A. Hewish, Structure and evolution of compound streams at ≤1 AU, *J. Geophys. Res.*, **96**, 21, 213, 1991.

24. B.V. Jackson, P.L. Hick, M. Kojima, and A. Yokobe, Heliospheric tomography using interplanetary scintillation observations, *Physics and Chemistry of the Earth*, **22**, No. 5, 425, 1997b.

25. B.V. Jackson, P.L. Hick, M. Kojima, and A. Yokobe, Heliospheric Tomography Using Interplanetary Scintillation Observations, for the COSPAR XXXI meeting held in Birmingham, England 14-21 July, 1996 *Adv. in Space Res.*, **20**, No. 1, 23, 1997c.
26. P. Hick, B.V. Jackson, R. and Schwenn, Synoptic Maps for the Heliospheric Thomson Scattering Brightness as Observed by the Helios Photometers, *Astron. Astrophys.* **285**, 1, 1990.
27. N.E. Hurlburt, P.C.H. Martens, and G.L. Slater, Volume reconstruction of magnetic fields using solar imagery, *ASP Conf. Series*, **68**, 30, 1994.
28. A.V. Panasyuk, Three-dimensional reconstruction of UV emissivities in the solar corona using Ultraviolet Coronagraph Spectrometer data from the Whole Sun Month, *J. Geophys. Res.,* **104**, 9721, 1999.
29. R.A. Frazin, Tomography of the solar corona. I. A robust, regularized, positive estimation method, *Astrophys. J.*, **530**, 1026, 2000.
30. R.A. Frazin, and P. Janzen, Tomography of the solar corona. II. Robust, regularized, positive estimation of the three-dimensional electron density distribution from LASCO-C2 polarized white-light images, *Astrophys. J.*, **570**, 408, 2002.
31. P.Z. Kunstz, A.S. Szalay, and A.R. Thakar, The hierarchical triangle mesh, in *Mining the Sky: Proc. of the MPA/ESO/MPE Workshop*, Garching; Banday, Zaroubi, and Bartlemann, (eds.), Springer-Verlag, Berlin, 631, 2001.
32. S.J. Tappin, A. Buffington, M.P. Cooke, C.J. Eyles, P.P. Hick, P.E. Holladay, B.V. Jackson, J.C. Johnston, T. Kuchar, D. Mizuno, J.B. Mozer, S. Price, R.R. Radick, G.M. Simnett, D. Sinclair, N.R. Waltham, and D.F. Webb, Tracking a Major Interplanetary Disturbance with SMEI, *Geophys. Res. Lett.* , **31**, 2802, 2004.

---

* bvjackson@ucsd.edu; phone 1 858 534-3358; fax 1 858 534-0177; http://casswww.ucsd.edu/solar/smei/index.html; mail code 0424, UCSD, 9500 Gilman Drive, La Jolla, CA 92093-0424
** abuffington@ucsd.edu; phone 1 858-534-6630; fax 1 858 534-7051;
*** pphick@ucsd.edu; phone 1 858 534-8965; fax 1 858 534-0177
**** x6wang@cs.ucsd.edu; 1 858 534-3358; fax 1 858 534-0177